Title

Correction to: Photoconversion changes bilin chromophore conjugation and protein secondary structure in the violet/orange cyanobacteriochrome NpF2163g3

Journal

Photochemical & Photobiological Sciences, 13(9)

ISSN

1474-905X

Authors

Lim, Sunghyuk
Rockwell, Nathan C
Martin, Shelley S
et al.

Publication Date

2014-09-01

DOI

10.1039/c4pp90025a

BIOCHEMISTRY
including biophysical chemistry & molecular biology

Article

pubs.acs.org/biochemistry

Characterization of Red/Green Cyanobacteriochrome NpR6012g4 by Solution Nuclear Magnetic Resonance Spectroscopy: A Hydrophobic Pocket for the C15-*E,anti* Chromophore in the Photoproduct

Nathan C. Rockwell,[†] Shelley S. Martin,[†] Sunghyuk Lim,[‡] J. Clark Lagarias,[†] and James B. Ames*[,‡]

[†]Department of Molecular and Cellular Biology and [‡]Department of Chemistry, University of California, Davis, California 95616, United States

Supporting Information

ABSTRACT: Cyanobacteriochromes (CBCRs) are cyanobacterial photosensory proteins distantly related to phytochromes. Like phytochromes, CBCRs reversibly photoconvert between a dark-stable state and a photoproduct via photoisomerization of the 15,16-double bond of their linear tetrapyrrole (bilin) chromophores. CBCRs provide cyanobacteria with complete coverage of the visible spectrum and near-ultraviolet region. One CBCR subfamily, the canonical red/green CBCRs typified by AnPixJg2 and NpR6012g4, can function as sensors of light color or intensity because of their great variation in photoproduct stability. The mechanistic basis for detection of green light by the photoproduct state in this subfamily has proven to be a challenging research topic, with competing hydration and trapped-twist models proposed. Here, we use ^{13}C-edited and ^{15}N-edited ^{1}H−^{1}H NOESY solution nuclear magnetic resonance spectroscopy to probe changes in chromophore configuration and protein−chromophore interactions in the NpR6012g4 photocycle. Our results confirm a C15-*Z,anti* configuration for the red-absorbing dark state and reveal a C15-*E,anti* configuration for the green-absorbing photoproduct. The photoactive chromophore D-ring is located in a hydrophobic environment in the photoproduct, surrounded by both aliphatic and aromatic residues. Characterization of variant proteins demonstrates that no aliphatic residue is essential for photoproduct tuning. Taken together, our results support the trapped-twist model over the hydration model for the red/green photocycle of NpR6012g4.

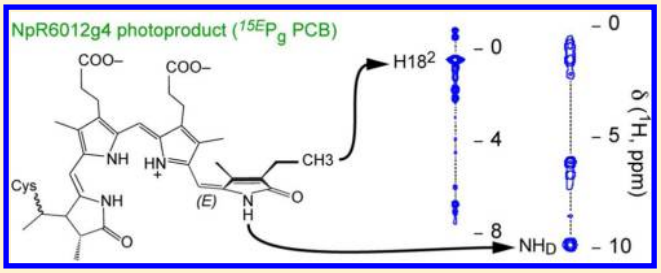

Photosynthetic organisms use photosensory proteins to optimize their metabolism in response to a wide range of photobiological cues. In addition to changes in light intensity during the diurnal cycle, such cues can also include the ambient color and transient changes in intensity caused by shading of a terrestrial organism or vertical mixing of a marine alga.[1−5] In cyanobacteria, changes in ambient color can give rise to changes in the light-harvesting phycobilisome antennae via processes such as CCA (complementary chromatic acclimation to green or red light) and FaRLiP (far-red-light photoacclimation).[6,7] Such processes are thought to be controlled by photoreceptors belonging to the phytochrome superfamily.[6−9] These cyanobacterial photosensors include not only red/far-red phytochromes related to those of land plants, fungi, other bacteria, and eukaryotic algae[10−13] but also distantly related cyanobacteriochrome (CBCR) photoreceptors.[14] FaRLiP is thought to be regulated by the red/far-red phytochrome RfpA, whereas CCA is regulated by the CBCRs CcaS or RcaE, depending on the species.[6−9] CBCRs also regulate phototaxis and biofilm formation in cyanobacteria,[15−21] and these photoreceptors provide complete coverage of the visible spectrum and the near-ultraviolet region.[14,22−25] CBCRs can also function as broadband sensors of light intensity.[25]

This spectral diversity makes phytochromes and CBCRs a tempting target for application in synthetic photobiology.[26−28] Because CBCRs exhibit such great diversity of photocycles, they hold the promise of allowing a researcher to quickly change the color sensitivity of a synthetic circuit or replace a color sensor with an intensity sensor. However, there remain several roadblocks for such applications. For example, general strategies for constructing CBCR-based synthetic systems are still being developed. There is also not a general approach for changing the color sensitivity of such systems, either by swapping the CBCR or by changing the color sensitivity of a given CBCR domain.[29] Advances on such problems require an improved understanding of the mechanisms these proteins use to detect given colors of light, to propagate the signal of light absorption within the CBCR, and to transduce that signal to the cell.

There are at least six CBCR subfamilies reported to date.[8,14,22,30−33] CBCRs and phytochromes both utilize covalently attached linear tetrapyrrole (bilin) chromophores to photoconvert between two photostates with distinct spectral properties.[10,11,34,35] Such proteins can thus sense the ratio between two spectral bands. Like phytochrome photocycles,

Received: April 22, 2015
Revised: May 19, 2015
Published: May 20, 2015

DOI: 10.1021/acs.biochem.5b00438
Biochemistry 2015, 54, 3772−3783

CBCR photocycles are driven by photoisomerization of the 15,16-double bond of the bilin chromophore between 15*Z* and 15*E* configurations.[22,24,36−42] However, CBCRs require only a single, isolated domain of ∼170 amino acids for autocatalytic chromophore assembly and full, reversible photoconversion.[14]

Known CBCRs typically bind phycocyanobilin (PCB) as a chromophore precursor. The initially produced CBCR holoprotein exhibits a dark-stable state having a 15*Z* bilin, with photoconversion yielding a photoproduct having a 15*E* bilin. Exceptional CBCRs can incorporate biliverdin as a chromophore precursor but exhibit the same pattern of photoisomerization.[43] Covalent protonated PCB adducts intrinsically absorb red and orange light in the 15*Z* and 15*E* configurations, respectively,[44] so CBCRs have evolved several tuning mechanisms for generating spectral diversity. For example, red/green CBCRs such as AnPixJg2,[30,41,45,46] Slr1393g3,[47,48] and NpR6012g4[25,49−52] exhibit a red-absorbing 15*Z* dark state and a green-absorbing 15*E* photoproduct (Figure 1A). The PCB chromophore is blue-shifted relative to the free chromophore in the photoproduct state of these CBCRs,[25,44,52] and this blue-shifting is proposed to arise due to trapping of the photoproduct chromophore in a twisted, sterically hindered geometry (Figure 1B).[52,53] Other models for this blue shift have also been proposed.[25,46] In particular, a recent study applying resonance Raman spectroscopy and molecular dynamics simulations to AnPixJg2 proposed that photoproduct tuning arose due to movement of a conserved "lid Trp" residue, followed by extensive solvation of the photoproduct.[46]

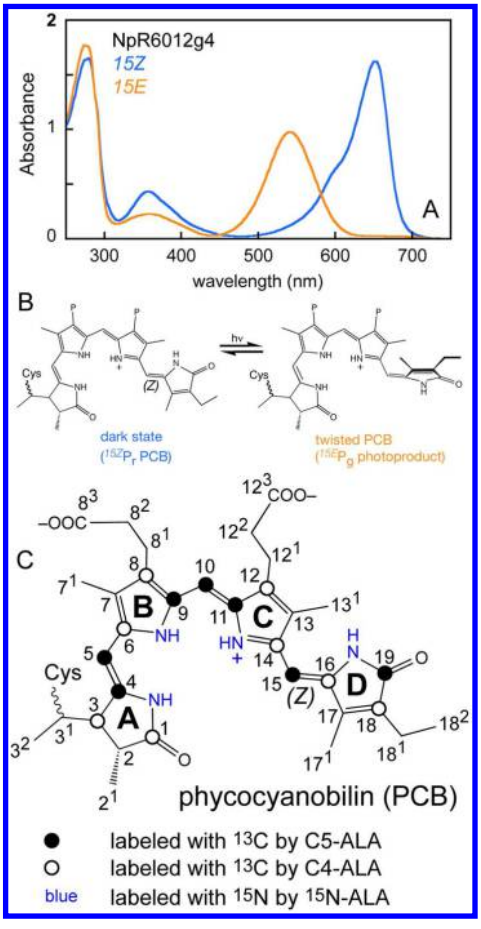

Figure 1. Trapped-twist red/green photocycle of NpR6012g4. (A) Absorption spectra of NpR6012g4 in the 15*Z* red-absorbing dark state (blue trace) and the 15*E* green-absorbing photoproduct (orange trace). (B) Structure of the phycocyanobilin (PCB) chromophore of NpR6012g4 in the proposed trapped-twist photocycle. (C) PCB numbering scheme for the dark state. Partial labeling patterns used in this study are indicated.

Work on spectral tuning of CBCRs has successfully elucidated changes in chromophore structure.[22−25,31,32,36,39,41,44−46,54,55] In some cases, specific amino acids have been identified as being essential for a given tuning mechanism or photocycle.[22−24,31,33,36,44,48,52] However, little is known about how protein−chromophore interactions change during photoconversion. Structural information for both photostates is available for only the blue/green CBCR TePixJ from *Thermosynechococcus elongatus*,[40−42] a member of the DXCF subfamily.[10,24,36] Secondary structure information is available for both photostates of the violet/orange CBCR NpF2164g3 from *Nostoc punctiforme*,[55,56] belonging to the inset-Cys subfamily.[22] Comparison of the NpF2164g3 secondary structure with that of TePixJ led to a proposed model for signal propagation.[55] Much less is known about other CBCR subfamilies, with only a crystal structure for AnPixJg2 in the dark state reported to date.[41] More information must be obtained if conserved signaling mechanisms are to be identified.

NpR6012g4 provides an attractive system for expanding our understanding of CBCR structure and function. It can be obtained in high yield, and it is known to exhibit exceptionally high quantum yields for primary photoisomerization compared to those of other phytochromes and CBCRs.[49−51,57,58] Extensive site-directed mutagenesis of this protein has identified residues that are important for spectral tuning of both photostates, including a conserved Phe residue (Phe634).[52] We have recently used a series of isotopically labeled NpR6012g4 samples (Figure 1C and Table S1 of the Supporting Information) to generate complete assignments of the C, H, and N atoms of the PCB chromophore in both photostates of NpR6012g4 (Tables S2 and S3 of the Supporting Information) using solution NMR spectroscopy.[59] This work established that the chromophore is protonated in both photostates, a result consistent with the trapped-twist model for photoproduct tuning. It also lays the groundwork for the study of protein−chromophore interactions and protein dynamics in NpR6012g4 using solution NMR techniques, ultimately leading to the determination of solution structures at atomic resolution.

Here, we have applied $^{1}H-^{1}H$ nuclear Overhauser effect spectroscopy (NOESY) to these isotopically labeled NpR6012g4 samples to examine chromophore configuration and protein−chromophore interactions. These studies confirm the C15-*Z*,*anti* configuration for the dark-state chromophore predicted by the AnPixJg2 crystal structure[41] and establish a C15-*E*,*anti* configuration for the photoproduct (Figure 1B). The photoproduct D-ring makes extensive close contacts with the protein in the photoproduct state, including contacts from the 18-ethyl group and the D-ring NH moiety to aliphatic and aromatic residues. Analysis of additional variant proteins containing single substitutions at aliphatic residues demonstrated that these residues are not essential for photoproduct tuning. Our studies support the trapped-twist model for photoproduct tuning and provide information that will ultimately lead to the determination of solution structures for NpR6012g4.

DOI: 10.1021/acs.biochem.5b00438
Biochemistry 2015, 54, 3772−3783

MATERIALS AND METHODS

Preparation of NpR6012g4. Expression, purification, and photoconversion of isotopically labeled NpR6012g4 have been described previously.[59] Variant proteins were constructed by site-directed mutagenesis using the QuikChange mutagenesis system (Stratagene) and the previously described NpR6012g4 intein−CBD fusion construct.[51,52] NpR6012g4 variants were recombinantly expressed in *Escherichia coli* engineered for coproduction of PCB[60] and were purified as previously described.[33,51,52] Purified variant proteins were characterized using absorbance spectroscopy and acid denaturation assays.[25,52,61,62] Photoconversion was triggered by illumination from above with a 75 W xenon source passed through a water filter and then through bandpass filters.[61] Bandpass filters used for triggering photochemistry were 650 nm (center) and 40 nm width (fwhm), 580 and 40 nm, 550 and 70 nm, and 500 and 25 nm. Purified protein was analyzed by SDS−PAGE using standard procedures and apparatus (Bio-Rad) followed by semidry transfer to PVDF membranes, staining with amido black for visualizing total protein, and zinc blotting[63] to confirm the presence of covalently bound bilin (Figure S1 of the Supporting Information).

NMR Spectroscopy. All NMR experiments were performed using a Bruker 600 MHz Avance III spectrometer equipped with a triple-resonance cryogenic TCI probe and pulsed field gradients,[55,56] with spectral acquisition at 298 K. NMR data were processed using the NMRPipe software package[64] and analyzed using SPARKY (www.cgl.ucsf.edu/home/sparky).

^{1}H−^{13}C and ^{1}H−^{15}N Correlation Spectroscopy. Bilin proton resonances attached to ^{13}C were selectively detected by isotope-edited correlation NMR experiments with WATERGATE solvent suppression.[65] The experimental parameters used for conventional ^{1}H−^{13}C and ^{1}H−^{15}N correlation NMR experiments have been described previously: ^{13}C(F2-edited) NOESY-HSQC,[66] ^{13}C(F2-edited and F3-filtered) NOESY-HSQC,[67] ^{15}N-edited NOESY-HSQC,[68] and ^{13}C(F1-edited)/^{15}N(F3-filtered) NOESY-HSQC.[66,67] The NOE mixing time in all ^{13}C/^{15}N-edited NOESY-HSQC experiments was 120 ms.

RESULTS

NOESY Analysis of the NpR6012g4 Dark State. We have previously determined complete assignments for the C, H, and N atoms of the NpR6012g4 chromophore in both photostates,[59] using a series of isotopically labeled samples (Tables S1−S3 of the Supporting Information). These assignments and samples allow the use of NOESY spectroscopy to probe the local environment of individual bilin H atoms using ^{13}C- or ^{15}N-edited ^{1}H−^{1}H NOESY spectroscopy. Intrachromophore interactions between bilin protons could be identified using the known chemical shifts of those protons (Table S3 of the Supporting Information) in combination with established edited and edited/filtered NOESY techniques.[66,67] We began with partially labeled samples (Figure 1C). These samples would potentially allow us to detect protons near H3 [C4-ALA labeling (Table S1 of the Supporting Information)], the three methine bridges (C5-ALA), and the four NH protons (^{15}N-ALA). For characterization of the 15*Z* dark state, the C5-ALA sample was exchanged into D_2O to avoid overlap of the water signal (4.8 ppm) with that of H15 (4.3 ppm). In the 15*Z* dark state, H3 exhibited NOESY cross-peaks to other A-ring protons (Figure 2A), to H5, and to protein resonances (Tables 1 and 2). H5 exhibited strong NOESY cross-peaks to H3^{2} and

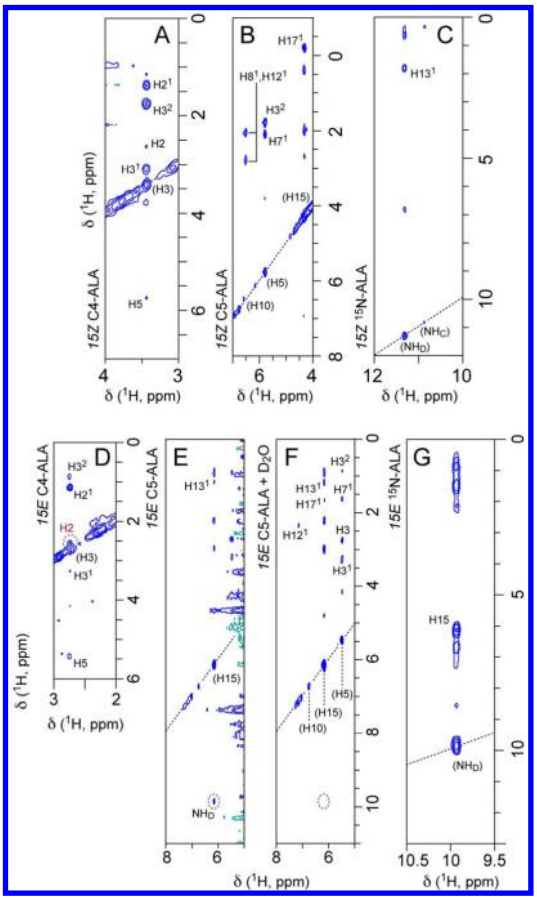

Figure 2. Assignment of ^{1}H−^{1}H NOESY contacts in partially labeled NpR6012g4 samples. (A) NpR6012g4 labeled with C4-ALA in the dark state. (B) NpR6012g4 labeled with C5-ALA in the dark state. (C) NpR6012g4 labeled with ^{15}N-ALA in the dark state. (D) NpR6012g4 labeled with C4-ALA in the photoproduct state. (E) NpR6012g4 labeled with C5-ALA in the photoproduct state. (F) NpR6012g4 labeled with C5-ALA in the photoproduct state, in D_2O. The circled resonance in panel E matches the chemical shift of NH_D and is lost upon D_2O exchange. (G) NpR6012g4 labeled with ^{15}N-ALA in the photoproduct state. Two-dimensional ^{15}N-edited NOESY-HSQC spectra used ^{15}N and ^{1}H (F_1 and F_2) carrier frequencies of 140 and 4.70 ppm and acquisition times of 25 (F_1) and 200 ms (F_2), respectively. Two-dimensional ^{13}C-edited NOESY-HSQC spectra used ^{13}C and ^{1}H (F_1 and F_2) carrier frequencies of 100 and 4.70 ppm and acquisition times of 25 (F_1) and 200 ms (F_2), respectively.

H7^{1} (Figure 2B), consistent with a C5-*Z*,*syn* configuration of the A- and B-rings (see Discussion). For H10, only cross-peaks to the bilin propionate side chains could be detected, whereas H15 exhibited robust cross-peaks both to H17^{1} and to several protein resonances (Figure 2B). The C-ring NH moiety exhibited a single cross-peak to an aliphatic protein proton (Figure 2C). NH_D exhibited cross-peaks to protein and/or water resonances and to H13^{1} on the C-ring (Figure 2C). The proximity of H13^{1} and NH_D is consistent with a C15-*Z*,*anti* configuration in the dark state (see Discussion).

We next performed two-dimensional (2D) ^{13}C-edited ^{1}H−^{1}H and ^{13}C-edited/^{13}C-filtered ^{1}H−^{1}H NOESY experiments on the globally labeled sample (Figure 3A). The combination of edited and edited/filtered spectra provided

DOI: 10.1021/acs.biochem.5b00438
Biochemistry 2015, 54, 3772−3783

Table 1. Intrachromophore NOESY Contacts in NpR6012g4

from[a]	H2	$H2^1$	H3	$H3^1$	$H3^2$	NH_A	H5	$H7^1$	8-12[b]	$H13^1$	H15	$H17^1$	$H18^1_a$	$H18^1_b$	$H18^2$	NH_D
H2		*Z,E*	*Z,E*	*Z*	*Z,E*											
$H2^1$	*Z,E*		*Z,E*	*Z,E*	*Z,E*	*Z*?	*Z,E*									
H3	*Z,E*	*Z,E*		*Z*	*Z,E*		*Z,E*	*Z*								
$H3^1$	*Z*	*Z*	*Z*		*Z*											
$H3^2$	*Z,E*	*Z,E*	*Z,E*	*Z,E*			*Z*	*Z*								
NH_A																
H5			*E*	*E*	*Z,E*			*Z,E*								
$H7^1$			*Z*,?		*Z*		*Z,E*		prop?							
8-12[b]									prop							
$H13^1$									prop			*E*				*Z*
H15										*E*		*Z,E*				*E*
$H17^1$										*E*	*Z,E*		*Z*,?	?,*E*	*Z,E*	
$H18^1_a$												*Z*,?		*Z,E*	*Z,E*	
$H18^1_b$												*E*	*Z,E*		*Z,E*	
$H18^2$												*Z,E*	*Z,E*	*Z,E*		
NH_D										*Z*	*E*					

[a]The left-hand column contains the atom on the diagonal of the NOESY strip; "*Z*" and "*E*" refer to NOESY cross-peaks in the dark-state and photoproduct spectra, respectively. Ambiguous assignments indicated with a question mark cannot be resolved because of similar ^{13}C shifts. [b]8-12 includes contacts to and from both propionates and H10; contacts to propionates are indicated by "prop" and are not reported in more detail.

Table 2. Chromophore–Protein Contacts in the NpR6012g4 Dark State

atom	NOESY cross-peak (ppm)																
$H2^1$	−0.8	0.3		0.8	0.95	1.2	2.2	2.4	3.9		4.4	4.8	5.8	7.0	7.3	10	12.2
H2		0.3									4.4						
$H3^2$		0.3	0.6		0.95				3.9	4.2	4.4	4.8					
H3						1.3	2.2		3.8								
H5									3.8								
$H7^1$						1.3			3.9	4.2		4.8		6.6			
NH_C	−0.2		0.5				2.1								7.1		
$H13^1$				0.7	1.0	1.6						4.8		6.8	7.3	8.9	
H15		0.4					2.0	2.7						7.0			
NH_D	−0.2		0.6											6.9			
$H17^1$					1.1				3.2						7.2	8.6	
$H18^1_a$															7.2		
$H18^1_b$															7.2		9.3
$H18^2$						1.6		2.4				4.7	5.6	6.5	7.2	8.7	9.3

information about potential cases in which protein–chromophore interactions and intrachromophore interactions overlapped. We used this information and the known C and H assignments (Tables S2 and S3 of the Supporting Information) to interpret the three-dimensional ^{13}C-edited $^1H-^1H$ NOESY spectra of the dark state (Figure 4). Extensive interactions were observed among the A-ring protons (H2, $H2^1$, H3, $H3^1$, and $H3^2$). $H2^1$ also exhibited weak cross-peaks potentially matching the chemical shifts of H5 and NH_A, but reciprocal contacts could not be detected; therefore, these interactions are not confirmed. Reciprocal cross-peaks were observed among $H3^1$, H2, and $H2^1$, but cross-peaks between $H3^1$ and H5 were not observed (Figures 2 and 4). These results are consistent with the stereochemistry of the covalent protein–chromophore linkage at $C3^1$ observed in the AnPixJg2 crystal structure.[41] Reciprocal cross-peaks from $H3^2$ and $H7^1$ to H5 were observed. $H7^1$ and $H13^1$ also exhibited cross-peaks to the propionate side chains, but the only cross-peaks observed from those side chains were cross-peaks between the nonequivalent $H8^2$ protons. Extensive protein–chromophore interactions were observed for $H2^1$, $H3^2$, $H7^1$, and $H13^1$. $H13^1$ also exhibited a reciprocal cross-peak to the D-ring NH. Multiple protein cross-peaks were detected for all D-ring side-chain protons ($H17^1$, $H18^2$, and the nonequivalent $H18^1$ protons). These protons also exhibited cross-peaks to each other. $H17^1$ exhibited a reciprocal cross-peak to H15, consistent with the C15-*Z,anti* configuration observed in the crystal structure of the related red/green CBCR AnPixJg2 in the dark state (see Discussion).[41]

NOESY Analysis of the NpR6012g4 Photoproduct. We next analyzed NOESY spectra for the NpR6012g4 photoproduct, beginning with partially labeled samples (Figure 2D–G and Figure S2 of the Supporting Information). H3 again exhibited cross-peaks to the other A-ring protons (Figure 2D). The cross-peak to H2 was partially overlapped by the diagonal signal from H3, but it was confirmed using a ^{13}C-edited/filtered $^1H-^1H$ NOESY spectrum (Figure S2A of the Supporting Information). Prior to D_2O exchange, no cross-peaks could be detected for the H5 and H10 methine protons (Figure 2E). Several cross-peaks to H15 were observed, including a downfield cross-peak matching the known chemical shift of the NH_D proton [9.9 ppm (Table S3 of the Supporting Information)]. Protein N atoms were labeled with ^{15}N in this sample (Table S1 of the Supporting Information), permitting further characterization of this resonance. The cross-peak at 9.9

DOI: 10.1021/acs.biochem.5b00438
Biochemistry 2015, 54, 3772–3783

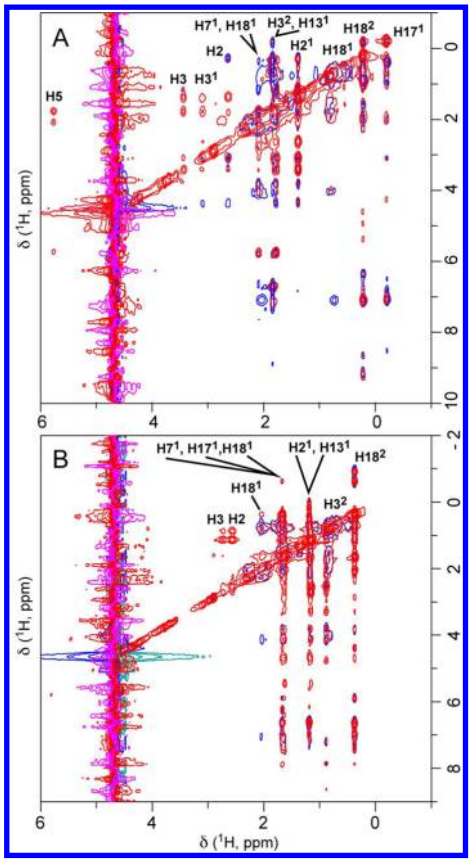

Figure 3. Characterization of NpR6012g4 using ^{13}C-edited ^{1}H−^{1}H NOESY. ^{13}C-edited (red/pink) and ^{13}C-edited, ^{13}C-filtered (blue/green) ^{1}H−^{1}H NOESY spectra are overlaid for the (A) dark state and (B) photoproduct. Both two-dimensional ^{13}C-edited NOESY-HSQC spectra and ^{13}C-edited/^{15}N,^{13}C(F2-filtered) NOESY-HSQC spectra were acquired with ^{15}N, ^{13}C, and ^{1}H (F_1 and F_2) carrier frequencies of 140, 40, and 4.70 ppm, respectively. The two-dimensional acquisition times were 25 (F_1) and 200 ms (F_2).

ppm was not suppressed in a ^{13}C-edited/^{15}N-filtered ^{1}H−^{1}H NOESY spectrum (Figure S2B of the Supporting Information) and was not observed in a ^{15}N-edited ^{1}H−^{1}H NOESY spectrum (Figure S2C of the Supporting Information), ruling out a protein NH proton. This cross-peak was lost on D_2O exchange (Figure 2F), ruling out a downfield CH proton. Moreover, a cross-peak from NH_D [9.9 ppm (Table S3 of the Supporting Information)] to H15 was observed (Figure 2G). Taken together, these results implicate the 9.9 ppm cross-peak from H15 as the NH_D proton and reveal reciprocal NOESY cross-peaks between H15 and NH_D in the NpR6012g4 photoproduct. The proximity of H15 and NH_D is consistent with a C15-*E*,*anti* configuration in the photoproduct (see Discussion).

We extended these results with 2D ^{13}C-edited/filtered and three-dimensional (3D) ^{13}C-edited ^{1}H−^{1}H NOESY experiments on the globally labeled photoproduct (Figures 3B and 5). A NOESY strip corresponding to the H3^1 proton was not detected. Cross-peaks to H3^1 were detected from H2^1 and H3^2, as in the dark state, but also from H5 (Figure 2F). The other A-ring protons exhibited cross-peaks to each other. H3 and H7^1 both exhibited cross-peaks to H5 (Figure 5), and reciprocal peaks were observed in the sample labeled with C5-ALA (Figure 2F). Extensive protein−chromophore cross-peaks were observed for H2^1 and H3^2 (Figure 5). H13^1 and H17^1 exhibit reciprocal cross-peaks in the photoproduct state, with H17^1 also exhibiting cross-peaks to the protons of the C18-ethyl side chain (Table 1). Extensive protein cross-peaks are seen for H13^1, H17^1, the 18-ethyl protons, and the D-ring NH proton (Figures 2G and 5 and Table 3). The proximity of H13^1 and H17^1 is once again consistent with a C15-*E*,*anti* configuration in the photoproduct (see Discussion).

Spectral Tuning of the NpR6012g4 Photoproduct Is Dominated by Aromatic Residues. NOESY cross-peaks to D-ring protons were detected for both aromatic and aliphatic protons [chemical shifts of ∼6−8 ppm and −2 to 3.5 ppm, respectively (Figure 5)]. Aromatic cross-peaks were expected for the dark state, given the proximity of Phe and Tyr residues to the bilin D-ring in the AnPixJ crystal structure.[41] Conserved Phe residues are essential for photoproduct tuning of red/green CBCRs,[33,52] consistent with the proximity of aromatic protons to the chromophore D-ring in the photoproduct. However, aliphatic residues have not been shown to be important for spectral tuning of the NpR6012g4 photoproduct.[52] We therefore used the AnPixJ crystal structure[41] to locate bulky aliphatic residues whose side chains were within 6 Å of the bilin D-ring (Figure 6). Five such residues were identified, corresponding to Leu660, Leu692, Val697, Ile702, and Leu714 in NpR6012g4. Variant proteins containing substitutions for Leu660 have been previously reported and do not exhibit effects on photoproduct tuning.[33,52] We also considered the possibility of a rearrangement on the α face of the bilin ring system (following the convention of refs 31, 61, and 69), consistent with the α-facial disposition of the chromophore D-ring in red/green CBCRs and with the variable effects of substitutions for His688.[25,51,52] These observations implicated Ile689 and Ile691 as other potentially relevant residues. We therefore constructed six variant proteins containing single substitutions (I_{689}A, I_{691}A, L_{692}A, V_{697}A, I_{702}A, and L_{714}F).

These variant proteins exhibited only slight effects on the peak absorption of either photostate (Figure 7 and Table 4). The characteristic red-shifted photoproduct absorption observed upon mutagenesis of Phe634 [F_{634}V variant (Table 4)][52] was not observed in any of these NpR6012g4 variants. Modest photoproduct red shifts were observed for I_{689}A and L_{714}F NpR6012g4 (Figure 7A,B). Slight photoproduct blue shifts were seen for I_{691}A, L_{692}A, and I_{702}A variant NpR6012g4 proteins (Figure 7C−E and Table 4). The photoproduct spectrum of V_{697}A NpR6012g4 was equivalent to that of wild-type NpR6012g4 (Figure 7F and Table 4). All of the observed photoproduct absorption maxima for these NpR6012g4 variants were within the observed range of photoproduct absorption maxima for wild-type red/green CBCRs (Figure 7, dashed lines, ref 25). We conclude that these aliphatic residues are not critical determinants for photoproduct tuning in NpR6012g4. Multiple substitutions at these positions could yet reveal a role in photoproduct tuning for the ensemble of aliphatic residues, and these residues could also be more important in other red/green CBCRs. By contrast, substitution of a smaller residue (Ala or Val) for Phe634 or its equivalent in the red/green CBCR NpR5113g2 resulted in significant photoproduct red shifts such that the photoproduct absorption maxima fall out of the observed "wild-type" range,[52] emphasizing the essential role for this residue in photoproduct tuning.

DISCUSSION

We have examined the red/green CBCR NpR6012g4 using NOESY spectroscopy. Our previous assignment of chromo-

DOI: 10.1021/acs.biochem.5b00438
Biochemistry 2015, 54, 3772−3783

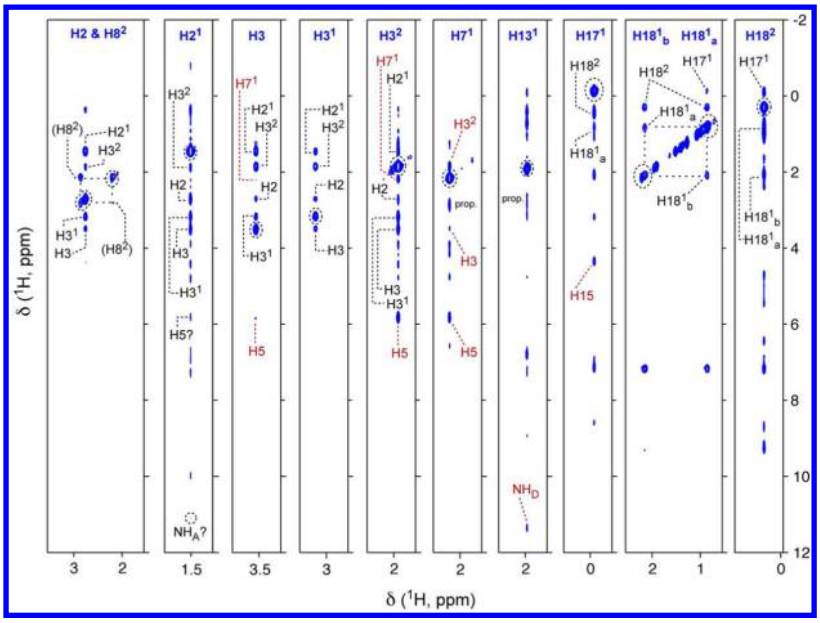

Figure 4. Characterization of the dark state using three-dimensional ^{13}C-edited ^{1}H−^{1}H NOESY. Strips are shown for the indicated PCB protons, with intrachromophore contacts indicated. Red highlights indicate contacts useful in assigning the configuration of the C5 and C15 methine bridges. The ^{13}C (F_2) and ^{1}H (F_1 and F_3) carrier frequencies were 40 and 4.70 ppm, respectively. The three-dimensional acquisition times were 25 (F_1), 10 (F_2), and 200 ms (F_3). Propionate side-chain peaks (prop) are not individually designated.

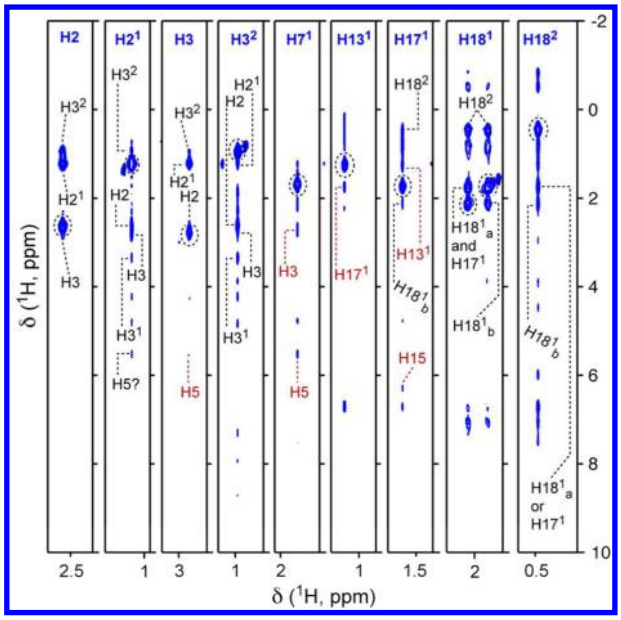

Figure 5. Characterization of the photoproduct using 3D ^{13}C-edited ^{1}H−^{1}H NOESY. Strips are shown for the indicated PCB protons, with intrachromophore contacts indicated. Spectral parameters and labeling are identical to those of Figure 4.

phore C, H, and N atoms[59] allows us to probe the environment of individual bilin protons, detecting both bilin−bilin and protein−bilin interactions. Both aliphatic and aromatic residues are found to be proximal to the D-ring in the photoproduct state, but aliphatic residues are not essential for photoproduct tuning. These studies provide constraints that define changes in chromophore configuration upon photoconversion and yield new information about protein−chromophore interactions during the red/green photocycle.

Chromophore Configuration in the NpR6012g4 Photocycle. The detected bilin−bilin H−H cross-peaks allow us to determine the configuration of the C5 and C15 chromophore methine bridges (Figure 8). Several interactions across these bridges are observed in both photostates (Figures 4and 5, red labels), and changes in these interactions also provide a direct demonstration of the chromophore geometry in the photoproduct. Across the C5 methine bridge, cross-peaks are observed from H3 to H5 and from H7^1 to H5 in both photostates (Figure 9). There are also cross-peaks from H7^1 to H3 and from H5 to H3^2 and H7^1 in both photostates, supporting the C5-*Z,syn* configuration for both photostates (Figure 8).

However, there are changes upon photoconversion in the observed cross-peaks at the A-ring. A reciprocal cross-peak between H7^1 and H3^2 is seen in the dark state but is absent in the photoproduct. There is also evidence of movement of the H3^1 proton, which exhibits cross-peaks from H2 and H3 only in the dark state. In the photoproduct state, H3^1 exhibits a cross-peak from H5 not observed in the dark state (Figure 9). These observations are consistent with rotation of the covalent linkage at C3^1 relative to the bilin A-ring about the C3−C3^1 bond, with concomitant rotation of the C3^2 methyl group and H3^1. The stereochemistry of the covalent linkage can also be inferred from the absence of an H5−H3^1 cross-peak and the presence of H2−H3^1 and H2^1−H3^1 cross-peaks in the dark state. These cross-peaks are consistent with the observed disposition of the reactive Cys residue and the C3 side chain in the AnPixJg2 crystal structure.[41]

The observed bilin−bilin NOESY cross-peaks across the C15 methine bridge provide direct evidence of photoisomerization of the 15,16-double bond of the bilin chromophore (Figure 10) and for a C15-*E,anti* chromophore configuration in the photoproduct (Figure 8B). Reciprocal H13^1−NH$_D$ and H15−H17^1 cross-peaks are seen in the 15*Z* dark state. These results are consistent with the C15-*Z,anti* configuration also seen in AnPixJg2[41] (Figure 8A). In the photoproduct, reciprocal H15−NH$_D$ and H13^1−H17^1 cross-peaks are observed. These interactions are consistent with a C15-*E,anti* configuration

DOI: 10.1021/acs.biochem.5b00438
Biochemistry 2015, 54, 3772−3783

Table 3. Chromophore−Protein Contacts in the NpR6012g4 Photoproduct

atom	NOESY cross-peak (ppm)																		
$H2^1$					0.8	1.5	1.7	1.9	2.3			4.3	4.8						
H2									2.3										
$H3^2$								1.9	2.3		3.9	4.2	4.8				7.3	7.9	8.7
H3												4.3							
H5												4.2							
$H7^1$						1.2							4.8						
$H13^1$				0.3	0.7				2.2						6.8				
H15									2.2	3.0			4.8						
NH_D					0.9	1.5			2.2						6.7	7.1			8.6
$H17^1$					0.8								4.8	6.2	6.8				
$H18^1{}_a$		−0.6			0.8						3.9				6.8	7.1			
$H18^1{}_b$	−0.9	−0.6			0.9										6.8	7.1			
$H18^2$	−0.9	−0.6			0.8	1.2				3.0	3.9	4.5		6.0	6.8	7.1	7.6		

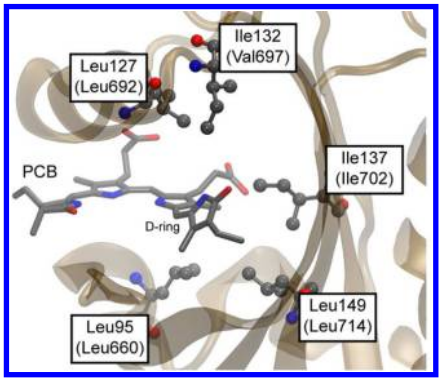

Figure 6. Identification of candidate aliphatic residues. The AnPixJg2 dark-state crystal structure (Protein Data Bank entry 3W2Z)[41] is shown. All Leu, Ile, Val, and Met residues within 6 Å of the chromophore D-ring or H15 are shown in ball-and-stick representation and labeled. Leu95, Leu127, Ile132, Ile137, and Leu149 correspond to Leu660, Leu692, Val697, Ile702, and Leu714 in NpR6012g4, respectively. This figure was prepared using VMD.[73]

(Figure 8B) rather than a C15-*E,syn* configuration. Interestingly, an H15−$H13^1$ cross-peak is observed in the photoproduct as well (Figure 10). This may arise due to twisting of the C15 methine bridge, as predicted by the trapped-twist model (Figure 1B). C15-*E,anti* geometries exhibit considerable twisting of the formal 14,15-single bond.[59] Moreover, *ab initio* calculations of such geometries show better agreement than with the experimental peak absorption of 15*E* NpR6012g4 than do equivalent calculations on C15-*E,syn* geometries.[59] We therefore assign the chromophore configuration in the NpR6012g4 photoproduct as twisted C15-*E,anti*, consistent with the original proposal of Narikawa, Ikeuchi, and colleagues.[30] Such a twisted C15-*E,anti* geometry is also sufficient to explain the characteristic photoproduct blue shift of NpR6012g4 and related CBCRs,[59] and our data do not provide unambiguous evidence of rotation about the other methine bridges. We therefore favor the minimal interpretation that the photoproduct chromophore adopts a C5-*Z,syn* C10-*Z,syn* C15-*E,anti* configuration in NpR6012g4.

Changing Protein−Chromophore Interactions in the NpR6012g4 Photocycle. The NOESY spectra also contain bilin−protein cross-peaks. Although we cannot yet identify the protein protons involved, their chemical shifts nevertheless provide information about the types of residues involved.[70] For example, side-chain C−H protons from aliphatic residues typically exhibit upfield chemical shifts of ≤3.5 ppm, whereas those from aromatic residues are typically downfield at 6−8 ppm. Thus, $H3^2$ exhibits probable cross-peaks to aliphatic protons in the dark state that are lost in the photoproduct, with the photoproduct $H3^2$ instead exhibiting cross-peaks to aromatic protons (Figure 9). Multiple protein−chromophore cross-peaks are lost at H2 and $H2^1$ upon photoproduct formation. Although this could be viewed as being caused by A-ring rotation, it is also consistent with movement of the A-ring and surrounding protein residues relative to each other. The latter hypothesis is supported by a similar loss of protein−chromophore cross-peaks on the B-ring at $H7^1$ and by retention of H5−$H3^2$ and H5−$H7^1$ cross-peaks upon photoconversion (Figure 8). The net loss of protein−chromophore interactions at the A- and B-rings in the photoproduct state would also seem to be inconsistent with trapping of a twisted A-ring configuration in this state.

Rotation about C10 is also consistent with the net loss of protein−chromophore interactions at the A- and B-rings and retention of configuration at C5. However, it is energetically disfavored relative to rotations about C5 and C15 in bilins with unsaturated C10 bridges.[71] Such a rotation would also require large-scale rearrangement of the surrounding protein, because the A-ring is covalently attached to the protein at $C3^1$ and the D-ring is more sterically crowded in red/green CBCRs than in phytochromes.[41,52] Moreover, such a rotation would be expected to have pronounced effects on the peak absorption of the chromophore. This study demonstrates formation of a C15-*E,anti* geometry in the photoproduct (see above), and such geometries are sufficient to explain the observed peak absorption without additional rotations.[59] We therefore conclude that movements about the C10 methine bridge are likely to be minor. The observed changes in protein−chromophore cross-peaks at the A- and B-rings thus would reflect movement of the chromophore relative to the surrounding protein (as in the flip-and-rotate model for phytochrome photoconversion)[38,72] and/or rotation of the covalent linkage at $C3^1$ relative to the chromophore A-ring.

Extensive changes in protein−chromophore cross-peaks are seen for the C- and D-rings (Figure 10). These include examples in which cross-peaks may be shifting upon photoconversion and examples in which cross-peaks appear or disappear upon photoconversion (Figure 10, magenta boxes). All three patterns can be seen for $H18^2$: peaks at 4−8 ppm could be shifting, but cross-peaks seen in the dark state at 8−10 ppm are lost upon photoconversion and peaks at −2 to 0 ppm appear upon photoconversion. Remarkably, several protein−

DOI: 10.1021/acs.biochem.5b00438
Biochemistry 2015, 54, 3772−3783

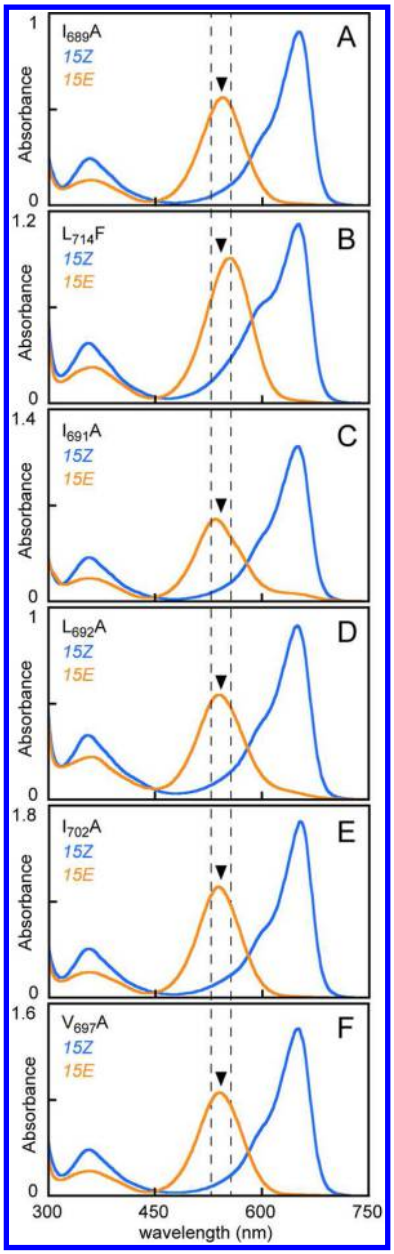

Figure 7. Characterization of variant NpR6012g4 proteins. (A) $I_{689}A$ NpR6012g4 is shown in the 15*Z* (blue) and 15*E* (orange) photostates. (B) $L_{714}F$ NpR6012g4 is shown in the color scheme of panel A. (C) $I_{691}A$ NpR6012g4 is shown in the color scheme of panel A. (D) $L_{692}A$ NpR6012g4 is shown in the color scheme of panel A. (E) $I_{702}A$ NpR6012g4 is shown in the color scheme of panel A. Vertical dashed lines indicate the observed range of photoproduct peak wavelengths for wild-type red/green CBCRs from *N. punctiforme* (528−556 nm),[25] and arrowheads indicate the wild-type peak wavelength for NpR6012g4 (Table 4).

Table 4. Characterization of NpR6012g4 Variant Proteins[a]

NpR6012g4 variant	15*Z* λ_{max} (nm)	15*E* λ_{max} (nm)	native SAR
none (wild-type)[b]	650	542	0.98
$F_{634}V$[b]	650	576	0.68
$I_{689}A$	652	544	1.17
$I_{691}A$	650	536	1.05
$L_{692}A$	650	538	0.48
$V_{697}A$	652	542	0.83
$I_{702}A$	654	538	0.99
$L_{714}F$	652	556	0.51

[a]SAR (specific absorbance ratio) was calculated as (peak red band absorption)/(peak 280 nm absorption). All peak wavelengths are derived from absorption spectra unless otherwise noted. [b]Value from ref 52.

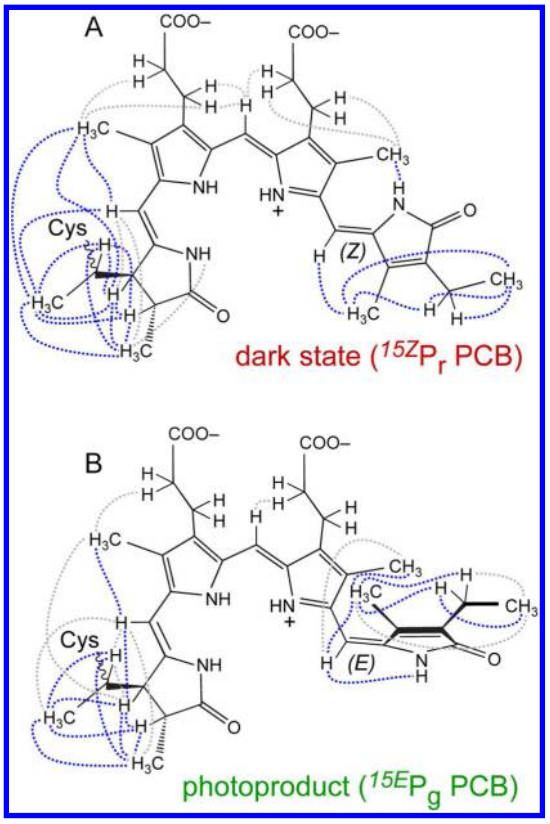

Figure 8. Changing bilin−bilin contacts in the NpR6012g4 photocycle. Intrachromophore contacts observed in ^{13}C-edited and ^{15}N-edited $^{1}H-^{1}H$ NOESY spectra are shown for the (A) dark state and (B) photoproduct. Reciprocally observed contacts are colored blue, whereas contacts observed in only one direction and contacts that are ambiguous because of spectral overlap are colored gray.

chromophore cross-peaks are observed for the D-ring NH proton. The detection of extensive NOESY cross-peaks for the photoproduct D-ring protons (Figure 10) is not consistent with a disordered, solvated chromophore binding pocket, because these protons should be in fast exchange in such an environment. Such rapidly exchanging protons would not be amenable to NOESY analysis, here performed with a mixing time of 120 ms. We readily observed both aliphatic and aromatic cross-peaks for NH_D, indicating that this moiety is in a hydrophobic environment with slow exchange. Aliphatic interactions are also seen for H15 and for the 18-ethyl side chain. Thus, the chromophore D-ring resides in a hydrophobic, slowly exchanging environment generated by both aliphatic and aromatic amino acids.

The proximity of the photoproduct D-ring to aromatic protons is not surprising, because Phe634 is essential for photoproduct tuning in NpR6012g4.[52] The equivalent Phe residue is also essential for proper photoproduct tuning in another red/green CBCR, NpR5113g2.[52] The proximity of aliphatic amino acids to the D-ring raised the possibility that such residues might also be essential for photoproduct tuning. However, none of the six aliphatic residues tested were essential for the formation of the green-absorbing photoproduct (Figure

DOI: 10.1021/acs.biochem.5b00438
Biochemistry 2015, 54, 3772−3783

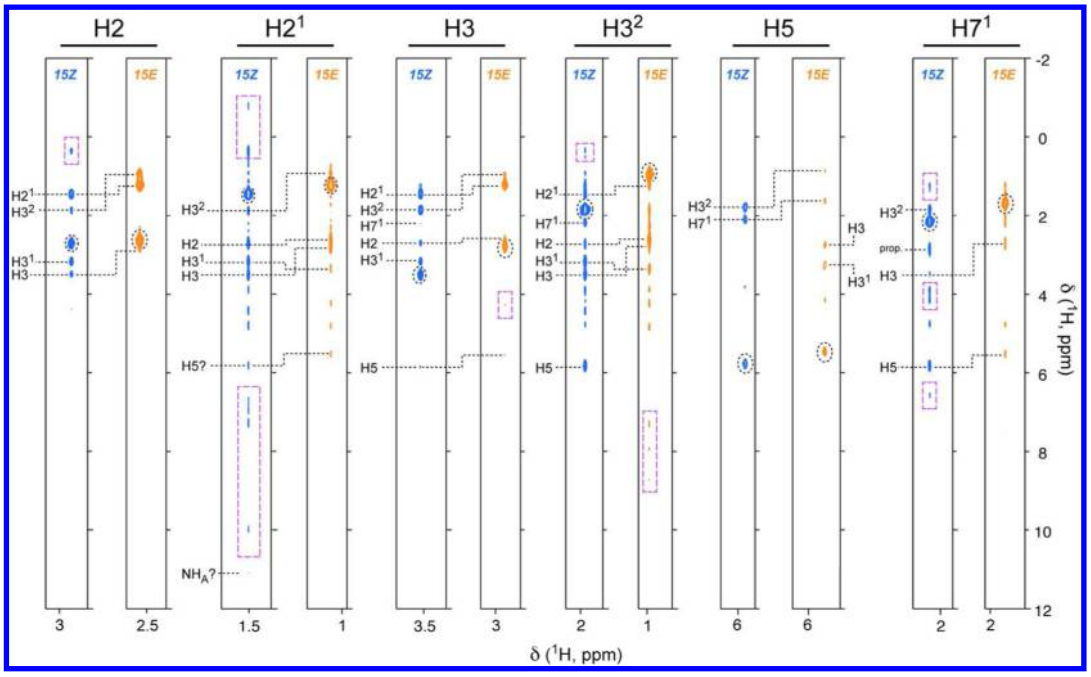

Figure 9. Changes in $^{1}H-^{1}H$ NOESY cross-peaks for A- and B-ring H atoms upon photoconversion. Strips are shown for individual PCB protons in the 15*Z* (blue) and 15*E* (orange) photostates. Bilin−bilin cross-peaks are indicated. Protein−chromophore interactions that appear or disappear upon photoconversion are highlighted (magenta boxes). Spectral parameters are identical to those given in Figure 2 (H15) or Figure 4 (all others).

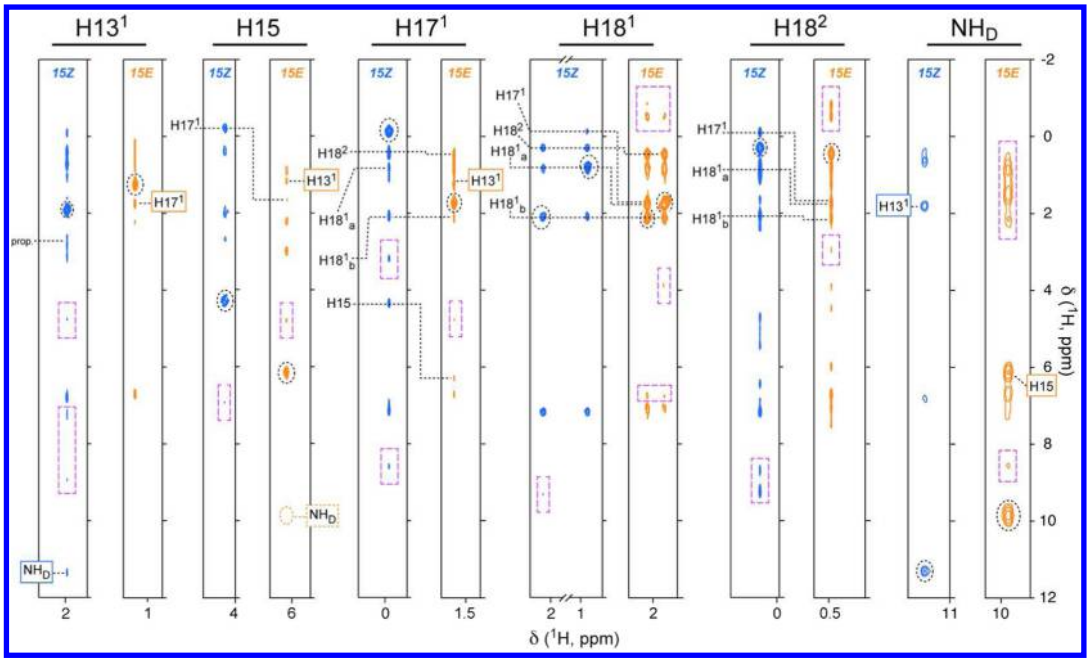

Figure 10. Changes in $^{1}H-^{1}H$ NOESY cross-peaks for C- and D-ring H atoms upon photoconversion. Strips are shown for individual PCB protons in the 15*Z* (blue) and 15*E* (orange) photostates. Bilin−bilin cross-peaks are indicated; boxed bilin−bilin contacts appear in only one photostate and were used to assign configuration of the C15 methine bridge. Protein−chromophore interactions that appear or disappear upon photoconversion are highlighted (magenta boxes). Spectral parameters are identical to those given in Figure 2 (H15) or Figure 4 (all others). H15 spectra are shown after D_2O exchange; the position of the NH_D cross-peak lost upon D_2O exchange is indicated.

7 and Table 4). In the absence of an atomic-resolution photoproduct structure, we cannot rule out rearrangement of the D-ring pocket such that some unknown residue becomes much closer to the chromophore in the photoproduct than it is in the dark state. However, Phe634 is essential for photoproduct tuning in NpR6012g4,[52] and the equivalent residue closely packs with the 18-ethyl side chain of PCB in the crystal structure of the AnPixJg2 dark state.[41] These observations implicate little to no movement of this residue upon photoconversion. Thus, at least part of the D-ring pocket does not seem to undergo dramatic restructuring. Our work supports the trapped-twist model for the red/green photocycle by demonstrating a hydrophobic, crowded environment for the photoproduct D-ring. The NMR NOESY assignments in this study (Tables 2 and 3) provide preliminary protein−chromophore data that will aid in the ultimate determination

DOI: 10.1021/acs.biochem.5b00438
Biochemistry 2015, 54, 3772−3783

of atomic-resolution solution structures for both photostates of NpR6012g4.

■ ASSOCIATED CONTENT

Supporting Information

Two figures and three tables. The Supporting Information is available free of charge on the ACS Publications website at DOI: 10.1021/acs.biochem.5b00438.

■ AUTHOR INFORMATION

Corresponding Author

*E-mail: jbames@ucdavis.edu.

Funding

This work was supported by a grant from the Chemical Sciences, Geosciences, and Biosciences Division, Office of Basic Energy Sciences, Office of Science, U.S. Department of Energy (DOE DE-FG02-09ER16117 to J.C.L. and J.B.A.).

Notes

The authors declare no competing financial interest.

■ ACKNOWLEDGMENTS

We thank Bennett Addison for help with NMR experiments and Jerry L. Dallas and Wolfgang Gärtner for helpful discussions.

■ ABBREVIATIONS

ALA, δ-aminolevulinic acid; ^{15}N-ALA, ALA labeled with ^{15}N; C4-ALA, ALA labeled with ^{13}C at the C4 position; C5-ALA, ALA labeled with ^{13}C at the C5 position; CBCR, cyanobacteriochrome; CCA, complementary chromatic acclimation; FaRLiP, far-red light photoacclimation; HSQC, heteronuclear single-quantum coherence; NMR, nuclear magnetic resonance; NOE, nuclear Overhauser effect; NOESY, NOE spectroscopy; PCB, phycocyanobilin; PVDF, polyvinylidene fluoride; SDS−PAGE, sodium dodecyl sulfate−polyacrylamide gel electrophoresis.

■ REFERENCES

(1) Franklin, K. A., and Quail, P. H. (2010) Phytochrome functions in *Arabidopsis* development. *J. Exp. Bot. 61*, 11−24.

(2) Casal, J. J. (2013) Photoreceptor signaling networks in plant responses to shade. *Annu. Rev. Plant Biol. 64*, 403−427.

(3) Rockwell, N. C., Lagarias, J. C., and Bhattacharya, D. (2014) Primary endosymbiosis and the evolution of light and oxygen sensing in photosynthetic eukaryotes. *Front. Ecol. Evol. 2*, DOI: 10.3389/fevo.2014.00066.

(4) Worden, A. Z., Lee, J. H., Mock, T., Rouze, P., Simmons, M. P., Aerts, A. L., Allen, A. E., Cuvelier, M. L., Derelle, E., Everett, M. V., Foulon, E., Grimwood, J., Gundlach, H., Henrissat, B., Napoli, C., McDonald, S. M., Parker, M. S., Rombauts, S., Salamov, A., Von Dassow, P., Badger, J. H., Coutinho, P. M., Demir, E., Dubchak, I., Gentemann, C., Eikrem, W., Gready, J. E., John, U., Lanier, W., Lindquist, E. A., Lucas, S., Mayer, K. F., Moreau, H., Not, F., Otillar, R., Panaud, O., Pangilinan, J., Paulsen, I., Piegu, B., Poliakov, A., Robbens, S., Schmutz, J., Toulza, E., Wyss, T., Zelensky, A., Zhou, K., Armbrust, E. V., Bhattacharya, D., Goodenough, U. W., Van de Peer, Y., and Grigoriev, I. V. (2009) Green evolution and dynamic adaptations revealed by genomes of the marine picoeukaryotes *Micromonas*. *Science 324*, 268−272.

(5) Karl, D. M., Church, M. J., Dore, J. E., Letelier, R. M., and Mahaffey, C. (2012) Predictable and efficient carbon sequestration in the North Pacific Ocean supported by symbiotic nitrogen fixation. *Proc. Natl. Acad. Sci. U.S.A. 109*, 1842−1849.

(6) Kehoe, D. M., and Gutu, A. (2006) Responding to color: The regulation of complementary chromatic adaptation. *Annu. Rev. Plant Biol. 57*, 127−150.

(7) Gan, F., Zhang, S., Rockwell, N. C., Martin, S. S., Lagarias, J. C., and Bryant, D. A. (2014) Extensive remodeling of a cyanobacterial photosynthetic apparatus in far-red light. *Science 345*, 1312−1317.

(8) Hirose, Y., Shimada, T., Narikawa, R., Katayama, M., and Ikeuchi, M. (2008) Cyanobacteriochrome CcaS is the green light receptor that induces the expression of phycobilisome linker protein. *Proc. Natl. Acad. Sci. U.S.A. 105*, 9528−9533.

(9) Hirose, Y., Narikawa, R., Katayama, M., and Ikeuchi, M. (2010) Cyanobacteriochrome CcaS regulates phycoerythrin accumulation in *Nostoc punctiforme*, a group II chromatic adapter. *Proc. Natl. Acad. Sci. U.S.A. 107*, 8854−8859.

(10) Rockwell, N. C., and Lagarias, J. C. (2010) A brief history of phytochromes. *ChemPhysChem 11*, 1172−1180.

(11) Auldridge, M. E., and Forest, K. T. (2011) Bacterial phytochromes: More than meets the light. *Crit. Rev. Biochem. Mol. Biol. 46*, 67−88.

(12) Duanmu, D., Bachy, C., Sudek, S., Wong, C. H., Jimenez, V., Rockwell, N. C., Martin, S. S., Ngan, C. Y., Reistetter, E. N., van Baren, M. J., Price, D. C., Wei, C. L., Reyes-Prieto, A., Lagarias, J. C., and Worden, A. Z. (2014) Marine algae and land plants share conserved phytochrome signaling systems. *Proc. Natl. Acad. Sci. U.S.A. 111*, 15827−15832.

(13) Rockwell, N. C., Duanmu, D., Martin, S. S., Bachy, C., Price, D. C., Bhattacharya, D., Worden, A. Z., and Lagarias, J. C. (2014) Eukaryotic algal phytochromes span the visible spectrum. *Proc. Natl. Acad. Sci. U.S.A. 111*, 3871−3876.

(14) Ikeuchi, M., and Ishizuka, T. (2008) Cyanobacteriochromes: A new superfamily of tetrapyrrole-binding photoreceptors in cyanobacteria. *Photochem. Photobiol. Sci. 7*, 1159−1167.

(15) Yoshihara, S., Suzuki, F., Fujita, H., Geng, X. X., and Ikeuchi, M. (2000) Novel putative photoreceptor and regulatory genes required for the positive phototactic movement of the unicellular motile cyanobacterium *Synechocystis* sp. PCC 6803. *Plant Cell Physiol. 41*, 1299−1304.

(16) Bhaya, D., Takahashi, A., and Grossman, A. R. (2001) Light regulation of type IV pilus-dependent motility by chemosensor-like elements in *Synechocystis* PCC6803. *Proc. Natl. Acad. Sci. U.S.A. 98*, 7540−7545.

(17) Bhaya, D. (2004) Light matters: Phototaxis and signal transduction in unicellular cyanobacteria. *Mol. Microbiol. 53*, 745−754.

(18) Yoshihara, S., Katayama, M., Geng, X., and Ikeuchi, M. (2004) Cyanobacterial Phytochrome-like PixJ1 Holoprotein Shows Novel Reversible Photoconversion Between Blue- and Green-absorbing Forms. *Plant Cell Physiol. 45*, 1729−1737.

(19) Narikawa, R., Suzuki, F., Yoshihara, S., Higashi, S. I., Watanabe, M., and Ikeuchi, M. (2011) Novel Photosensory Two-Component System (PixA-NixB-NixC) Involved in the Regulation of Positive and Negative Phototaxis of Cyanobacterium *Synechocystis* sp. PCC 6803. *Plant Cell Physiol. 52*, 2214−2224.

(20) Song, J. Y., Cho, H. S., Cho, J. I., Jeon, J. S., Lagarias, J. C., and Park, Y. I. (2011) Near-UV cyanobacteriochrome signaling system elicits negative phototaxis in the cyanobacterium *Synechocystis* sp. PCC 6803. *Proc. Natl. Acad. Sci. U.S.A. 108*, 10780−10785.

(21) Enomoto, G., Nomura, R., Shimada, T., Win, N. N., Narikawa, R., and Ikeuchi, M. (2014) Cyanobacteriochrome SesA is a diguanylate cyclase that induces cell aggregation in *Thermosynechococcus*. *J. Biol. Chem. 289*, 24801−24809.

(22) Rockwell, N. C., Martin, S. S., Feoktistova, K., and Lagarias, J. C. (2011) Diverse two-cysteine photocycles in phytochromes and cyanobacteriochromes. *Proc. Natl. Acad. Sci. U.S.A. 108*, 11854−11859.

(23) Enomoto, G., Hirose, Y., Narikawa, R., and Ikeuchi, M. (2012) Thiol-based photocycle of the blue and teal light-sensing cyanobacteriochrome Tlr1999. *Biochemistry 51*, 3050−3058.

(24) Rockwell, N. C., Martin, S. S., Gulevich, A. G., and Lagarias, J. C. (2012) Phycoviolobilin formation and spectral tuning in the DXCF cyanobacteriochrome subfamily. *Biochemistry 51*, 1449−1463.

DOI: 10.1021/acs.biochem.5b00438
Biochemistry 2015, 54, 3772−3783

(25) Rockwell, N. C., Martin, S. S., and Lagarias, J. C. (2012) Red/Green Cyanobacteriochromes: Sensors of Color and Power. *Biochemistry 51*, 9667−9677.
(26) Möglich, A., and Moffat, K. (2010) Engineered photoreceptors as novel optogenetic tools. *Photochem. Photobiol. Sci. 9*, 1286−1300.
(27) Tabor, J. J., Levskaya, A., and Voigt, C. A. (2011) Multichromatic Control of Gene Expression in *Escherichia coli*. *J. Mol. Biol. 405*, 315−324.
(28) Müller, K., and Weber, W. (2013) Optogenetic tools for mammalian systems. *Mol. BioSyst. 9*, 596−608.
(29) Rockwell, N. C., Martin, S. S., and Lagarias, J. C. (2015) Identification of DXCF cyanobacteriochrome lineages with predictable photocycles. *Photochem. Photobiol. Sci. 14*, 929−941.
(30) Narikawa, R., Fukushima, Y., Ishizuka, T., Itoh, S., and Ikeuchi, M. (2008) A novel photoactive GAF domain of cyanobacteriochrome AnPixJ that shows reversible green/red photoconversion. *J. Mol. Biol. 380*, 844−855.
(31) Rockwell, N. C., Njuguna, S. L., Roberts, L., Castillo, E., Parson, V. L., Dwojak, S., Lagarias, J. C., and Spiller, S. C. (2008) A second conserved GAF domain cysteine is required for the blue/green photoreversibility of cyanobacteriochrome Tlr0924 from *Thermosynechococcus elongatus*. *Biochemistry 47*, 7304−7316.
(32) Narikawa, R., Enomoto, G., Ni Ni, W., Fushimi, K., and Ikeuchi, M. (2014) A New Type of Dual-Cys Cyanobacteriochrome GAF Domain Found in Cyanobacterium *Acaryochloris marina*, Which Has an Unusual Red/Blue Reversible Photoconversion Cycle. *Biochemistry 53*, 5051−5059.
(33) Rockwell, N. C., Martin, S. S., Gan, F., Bryant, D. A., and Lagarias, J. C. (2015) NpR3784 is the prototype for a distinctive group of red/green cyanobacteriochromes using alternative Phe residues for photoproduct tuning. *Photochem. Photobiol. Sci. 14*, 258−269.
(34) Rockwell, N. C., Su, Y. S., and Lagarias, J. C. (2006) Phytochrome structure and signaling mechanisms. *Annu. Rev. Plant Biol. 57*, 837−858.
(35) Hughes, J. (2010) Phytochrome three-dimensional structures and functions. *Biochem. Soc. Trans. 38*, 710−716.
(36) Ishizuka, T., Kamiya, A., Suzuki, H., Narikawa, R., Noguchi, T., Kohchi, T., Inomata, K., and Ikeuchi, M. (2011) The cyanobacteriochrome, TePixJ, isomerizes its own chromophore by converting phycocyanobilin to phycoviolobilin. *Biochemistry 50*, 953−961.
(37) Song, C., Psakis, G., Lang, C., Mailliet, J., Gartner, W., Hughes, J., and Matysik, J. (2011) Two ground state isoforms and a chromophore D-ring photoflip triggering extensive intramolecular changes in a canonical phytochrome. *Proc. Natl. Acad. Sci. U.S.A. 108*, 3842−3847.
(38) Yang, X., Ren, Z., Kuk, J., and Moffat, K. (2011) Temperature-scan cryocrystallography reveals reaction intermediates in bacteriophytochrome. *Nature 479*, 428−432.
(39) Rockwell, N. C., Martin, S. S., and Lagarias, J. C. (2012) Mechanistic Insight into the Photosensory Versatility of DXCF Cyanobacteriochromes. *Biochemistry 51*, 3576−3585.
(40) Burgie, E. S., Walker, J. M., Phillips, G. N., Jr., and Vierstra, R. D. (2013) A photo-labile thioether linkage to phycoviolobilin provides the foundation for the blue/green photocycles in DXCF-cyanobacteriochromes. *Structure 21*, 88−97.
(41) Narikawa, R., Ishizuka, T., Muraki, N., Shiba, T., Kurisu, G., and Ikeuchi, M. (2013) Structures of cyanobacteriochromes from phototaxis regulators AnPixJ and TePixJ reveal general and specific photoconversion mechanism. *Proc. Natl. Acad. Sci. U.S.A. 110*, 918−923.
(42) Cornilescu, C. C., Cornilescu, G., Burgie, E. S., Markley, J. L., Ulijasz, A. T., and Vierstra, R. D. (2014) Dynamic structural changes underpin photoconversion of a blue/green cyanobacteriochrome between its dark and photoactivated states. *J. Biol. Chem. 289*, 3055−3065.
(43) Narikawa, R., Nakajima, T., Aono, Y., Fushimi, K., Enomoto, G., Ni Ni, W., Itoh, S., Sato, M., and Ikeuchi, M. (2015) A biliverdin-binding cyanobacteriochrome from the chlorophyll d-bearing cyanobacterium *Acaryochloris marina*. *Sci. Rep. 5*, 7950.
(44) Hirose, Y., Rockwell, N. C., Nishiyama, K., Narikawa, R., Ukaji, Y., Inomata, K., Lagarias, J. C., and Ikeuchi, M. (2013) Green/red cyanobacteriochromes regulate complementary chromatic acclimation via a protochromic photocycle. *Proc. Natl. Acad. Sci. U.S.A. 110*, 4974−4979.
(45) Fukushima, Y., Iwaki, M., Narikawa, R., Ikeuchi, M., Tomita, Y., and Itoh, S. (2011) Photoconversion mechanism of a green/red photosensory cyanobacteriochrome AnPixJ: Time-resolved optical spectroscopy and FTIR analysis of the AnPixJ-GAF2 domain. *Biochemistry 50*, 6328−6339.
(46) Velazquez Escobar, F., Utesch, T., Narikawa, R., Ikeuchi, M., Mroginski, M. A., Gartner, W., and Hildebrandt, P. (2013) Photoconversion Mechanism of the Second GAF Domain of Cyanobacteriochrome AnPixJ and the Cofactor Structure of Its Green-Absorbing State. *Biochemistry 52*, 4871−4880.
(47) Chen, Y., Zhang, J., Luo, J., Tu, J. M., Zeng, X. L., Xie, J., Zhou, M., Zhao, J. Q., Scheer, H., and Zhao, K. H. (2012) Photophysical diversity of two novel cyanobacteriochromes with phycocyanobilin chromophores: Photochemistry and dark reversion kinetics. *FEBS J. 279*, 40−54.
(48) Xu, X. L., Gutt, A., Mechelke, J., Raffelberg, S., Tang, K., Miao, D., Valle, L., Borsarelli, C. D., Zhao, K. H., and Gärtner, W. (2014) Combined mutagenesis and kinetics characterization of the bilin-binding GAF domain of the protein Slr1393 from the Cyanobacterium *Synechocystis* PCC6803. *ChemBioChem 15*, 1190−1199.
(49) Kim, P. W., Freer, L. H., Rockwell, N. C., Martin, S. S., Lagarias, J. C., and Larsen, D. S. (2012) Second-Chance Initiation Dynamics of the Cyanobacterial Photocycle in the NpR6012 GAF4 Domain of *Nostoc punctiforme*. *J. Am. Chem. Soc. 134*, 130−133.
(50) Kim, P. W., Freer, L. H., Rockwell, N. C., Martin, S. S., Lagarias, J. C., and Larsen, D. S. (2012) Femtosecond Photodynamics of the Red/Green Cyanobacteriochrome NpR6012g4 from *Nostoc punctiforme*. 2. Reverse Dynamics. *Biochemistry 51*, 619−630.
(51) Kim, P. W., Freer, L. H., Rockwell, N. C., Martin, S. S., Lagarias, J. C., and Larsen, D. S. (2012) Femtosecond Photodynamics of the Red/Green Cyanobacteriochrome NpR6012g4 from *Nostoc punctiforme*. 1. Forward Dynamics. *Biochemistry 51*, 608−618.
(52) Rockwell, N. C., Martin, S. S., Gulevich, A. G., and Lagarias, J. C. (2014) Conserved phenylalanine residues are required for blue-shifting of cyanobacteriochrome photoproducts. *Biochemistry 53*, 3118−3130.
(53) Narikawa, R., Kohchi, T., and Ikeuchi, M. (2008) Characterization of the photoactive GAF domain of the CikA homolog (SyCikA, Slr1969) of the cyanobacterium *Synechocystis* sp. PCC 6803. *Photochem. Photobiol. Sci. 7*, 1253−1259.
(54) Ishizuka, T., Narikawa, R., Kohchi, T., Katayama, M., and Ikeuchi, M. (2007) Cyanobacteriochrome TePixJ of *Thermosynechococcus elongatus* harbors phycoviolobilin as a chromophore. *Plant Cell Physiol. 48*, 1385−1390.
(55) Lim, S., Rockwell, N. C., Martin, S. S., Dallas, J. L., Lagarias, J. C., and Ames, J. B. (2014) Photoconversion changes bilin chromophore conjugation and protein secondary structure in the violet/orange cyanobacteriochrome NpF2163g3. *Photochem. Photobiol. Sci. 13*, 951−962.
(56) Lim, S., Rockwell, N. C., Martin, S. S., Lagarias, J. C., and Ames, J. B. (2014) ^{1}H, ^{15}N, and ^{13}C chemical shift assignments of cyanobacteriochrome NpF2164g3 in the photoproduct state. *Biomol. NMR Assignments 8*, 259−262.
(57) Chang, C. W., Gottlieb, S. M., Kim, P. W., Rockwell, N. C., Lagarias, J. C., and Larsen, D. S. (2013) Reactive ground-state pathways are not ubiquitous in red/green cyanobacteriochromes. *J. Phys. Chem. B 117*, 11229−11238.
(58) Gottlieb, S. M., Kim, P. W., Chang, C. W., Hanke, S. J., Hayer, R. J., Rockwell, N. C., Martin, S. S., Lagarias, J. C., and Larsen, D. S. (2015) Conservation and diversity in the primary forward photodynamics of red/green cyanobacteriochromes. *Biochemistry 54*, 1028−1042.
(59) Rockwell, N. C., Martin, S. S., Lim, S., Lagarias, J. C., and Ames, J. B. (2015) Characterization of red/green cyanobacteriochrome NpR6012g4 by solution nuclear magnetic resonance spectroscopy: A

DOI: 10.1021/acs.biochem.5b00438
Biochemistry 2015, 54, 3772−3783

protonated bilin ring system in both photostates. *Biochemistry 54*, 2581−2600.
(60) Gambetta, G. A., and Lagarias, J. C. (2001) Genetic engineering of phytochrome biosynthesis in bacteria. *Proc. Natl. Acad. Sci. U.S.A. 98*, 10566−10571.
(61) Rockwell, N. C., Shang, L., Martin, S. S., and Lagarias, J. C. (2009) Distinct classes of red/far-red photochemistry within the phytochrome superfamily. *Proc. Natl. Acad. Sci. U.S.A. 106*, 6123−6127.
(62) Shang, L., Rockwell, N. C., Martin, S. S., and Lagarias, J. C. (2010) Biliverdin amides reveal roles for propionate side chains in bilin reductase recognition and in holophytochrome assembly and photoconversion. *Biochemistry 49*, 6070−6082.
(63) Berkelman, T. R., and Lagarias, J. C. (1986) Visualization of bilin-linked peptides and proteins in polyacrylamide gels. *Anal. Biochem. 156*, 194−201.
(64) Delaglio, F., Grzesiek, S., Vuister, G. W., Zhu, G., Pfeifer, J., and Bax, A. (1995) NMRPipe: A multidimensional spectral processing system based on UNIX pipes. *J. Biomol. NMR 6*, 277−293.
(65) Piotto, M., Saudek, V., and Sklenar, V. (1992) Gradient-tailored excitation for single-quantum NMR spectroscopy of aqueous solutions. *J. Biomol. NMR 2*, 661−665.
(66) Ikura, M., Spera, S., Barbato, G., Kay, L. E., Krinks, M., and Bax, A. (1991) Secondary structure and side-chain ^{1}H and ^{13}C resonance assignments of calmodulin in solution by heteronuclear multidimensional NMR spectroscopy. *Biochemistry 30*, 9216−9228.
(67) Lee, W., Revington, M. J., Arrowsmith, C., and Kay, L. E. (1994) A pulsed field gradient isotope-filtered 3D ^{13}C HMQC-NOESY experiment for extracting intermolecular NOE contacts in molecular complexes. *FEBS Lett. 350*, 87−90.
(68) Marion, D., Driscoll, P. C., Kay, L. E., Wingfield, P. T., Bax, A., Gronenborn, A. M., and Clore, G. M. (1989) Overcoming the overlap problem in the assignment of ^{1}H NMR spectra of larger proteins by use of three-dimensional heteronuclear ^{1}H-^{15}N Hartmann-Hahn-multiple quantum coherence and nuclear Overhauser-multiple quantum coherence spectroscopy: Application to interleukin 1 *β*. *Biochemistry 28*, 6150−6156.
(69) Rose, I. A., Hanson, K. R., Wilkinson, K. D., and Wimmer, M. J. (1980) A suggestion for naming faces of ring compounds. *Proc. Natl. Acad. Sci. U.S.A. 77*, 2439−2441.
(70) Schwarzinger, S., Kroon, G. J., Foss, T. R., Wright, P. E., and Dyson, H. J. (2000) Random coil chemical shifts in acidic 8 M urea: Implementation of random coil shift data in NMRView. *J. Biomol. NMR 18*, 43−48.
(71) Falk, H. (1989) *The Chemistry of Linear Oligopyrroles and Bile Pigments*, Springer-Verlag, Vienna.
(72) Yang, X., Kuk, J., and Moffat, K. (2009) Conformational differences between the Pfr and Pr states in *Pseudomonas aeruginosa* bacteriophytochrome. *Proc. Natl. Acad. Sci. U.S.A. 106*, 15639−15644.
(73) Humphrey, W., Dalke, A., and Schulten, K. (1996) VMD: Visual molecular dynamics. *J. Mol. Graphics 14*, 33−38.

DOI: 10.1021/acs.biochem.5b00438
Biochemistry 2015, 54, 3772−3783